

RESEARCH ARTICLE

# Depolarization of intense laser beams by dynamic plasma density gratings

Y. X. Wang<sup>1,2</sup>, S. M. Weng<sup>1,2</sup>, P. Li<sup>3</sup>, Z. C. Shen<sup>3</sup>, X. Y. Jiang<sup>1,2</sup>, J. Huang<sup>1,2</sup>, X. L. Zhu<sup>1,2</sup>,  
H. H. Ma<sup>1,2</sup>, X. B. Zhang<sup>1,2,4</sup>, X. F. Li<sup>1,2</sup>, Z. M. Sheng<sup>1,2,5</sup>, and J. Zhang<sup>1,2,5</sup>

<sup>1</sup>Key Laboratory for Laser Plasmas (MoE), School of Physics and Astronomy, Shanghai Jiao Tong University, Shanghai, China

<sup>2</sup>Collaborative Innovation Center of IFSA, Shanghai Jiao Tong University, Shanghai, China

<sup>3</sup>Research Center of Laser Fusion of China Academy of Engineering Physics, Mianyang, China

<sup>4</sup>College of Physics and Electronics Engineering, Northwest Normal University, Lanzhou, China

<sup>5</sup>Tsung-Dao Lee Institute, Shanghai Jiao Tong University, Shanghai, China

(Received 29 August 2022; revised 16 January 2023; accepted 20 February 2023)

## Abstract

As a typical plasma-based optical element that can sustain ultra-high light intensity, plasma density gratings driven by intense laser pulses have been extensively studied for wide applications. Here, we show that the plasma density grating driven by two intersecting driver laser pulses is not only nonuniform in space but also varies over time. Consequently, the probe laser pulse that passes through such a dynamic plasma density grating will be depolarized, that is, its polarization becomes spatially and temporally variable. More importantly, the laser depolarization may spontaneously take place for crossed laser beams if their polarization angles are arranged properly. The laser depolarization by a dynamic plasma density grating may find application in mitigating parametric instabilities in laser-driven inertial confinement fusion.

**Keywords:** depolarization; high-power laser; plasma density grating

## 1. Introduction

With the development of laser technology, especially the invention of the chirped-pulse amplification (CPA) technique<sup>[1]</sup>, laser peak power and focused intensity have been increasing dramatically<sup>[2,3]</sup>. Simultaneously, intense laser-matter interactions have attracted great interest since they not only promise wide potential applications but also give birth to rich physical phenomena<sup>[4,5]</sup>. With the increase of laser power, however, the generation and manipulation of intense laser pulses have become more and more challenging due to the limited damage threshold of traditional optical devices<sup>[6]</sup>. In contrast, plasma-based optical elements can sustain ultra-high light intensity and hence provide an

alternative approach to the generation and manipulation of intense lasers.

In the last decades, plasma optics has developed into an attractive methodology for the manipulation and further amplification of intense lasers. For example, plasma mirrors have been widely used to enhance the contrast of intense laser pulses<sup>[7]</sup> or tightly focus laser pulses toward extreme intensities<sup>[8]</sup>. More significantly, both stimulated Raman and Brillouin scatterings in plasmas could be employed to amplify intense laser pulses<sup>[9–12]</sup>. Moreover, magnetized plasmas may have some specific advantages in the control and amplification of intense laser pulses<sup>[13–16]</sup>. Further, holographic plasma lenses have recently been proposed as a novel plasma optical device for broad applications<sup>[17–19]</sup>. In particular, laser-induced plasma density gratings (PDGs) have been extensively studied and proposed for wide potential applications, including the temporal compression, polarization control and manipulation of intense laser pulses<sup>[20–25]</sup>. Analogously, laser-induced plasma density modulations can tune laser power distribution to achieve

Correspondence to: S. M. Weng and Z. M. Sheng, Key Laboratory for Laser Plasmas (MoE), School of Physics and Astronomy, Shanghai Jiao Tong University, Shanghai 200240, China. Email: [wengsuming@sjtu.edu.cn](mailto:wengsuming@sjtu.edu.cn) (S. M. Weng); [zmsheng@sjtu.edu.cn](mailto:zmsheng@sjtu.edu.cn) (Z. M. Sheng). P. Li, Research Center of Laser Fusion of China Academy of Engineering Physics, Mianyang 621900, China. Email: [liping1984@caep.cn](mailto:liping1984@caep.cn) (P. Li)

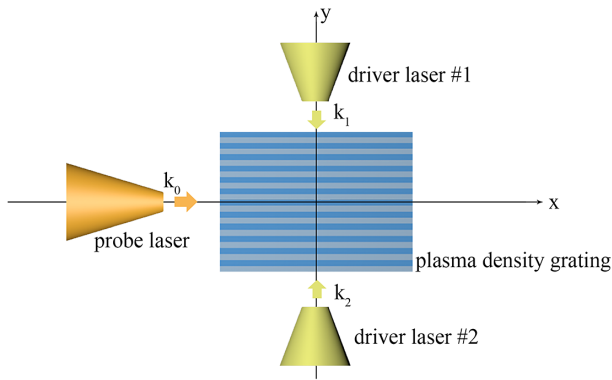


**Figure 1.** Schematic of laser depolarization by a PDG. The PDG driven by intersecting laser pulses #1 and #2 will be nonuniform in the  $y$  direction and also time-dependent. After the probe laser pulse passes through such a PDG, its polarization state will become nonuniform and time-dependent.

a symmetric inertial confinement fusion (ICF) implosion in the so-called crossed-beam energy transfer<sup>[26–28]</sup>.

In this paper, we investigate the spatial and temporal distributions of the polarization state of a probe laser pulse after it passes through a PDG. As shown in Figure 1, the PDG is driven by two intersecting laser pulses that have Gaussian intensity profiles in both the longitudinal and transverse directions. Due to the birefringence caused by the PDG, it could be employed as a waveplate for an ultrashort laser pulse. In this study, however, the formed PDG is not only nonuniform in space but also varies over time. Therefore, the refractive index modulation induced by such a PDG will be nonuniform and time-dependent. As a result, the probe laser pulse may be depolarized by such a dynamic PDG, that is, its polarization state becomes variable in both space and time. The laser beams with varying polarization states may play an important role in mitigating parametric instabilities in laser–plasma interactions relevant to ICF<sup>[29,30]</sup>. The paper is organized as follows. The formation and evolution of the PDG are simulated and analyzed in Section 2. The laser depolarization by the dynamic PDG is illustrated in Section 3. Finally, the conclusion and some discussions are presented in Section 4.

## 2. Dynamics of the plasma density grating

To understand the depolarization of laser beams, we first investigate the dynamics of the PDG, which can be well described by the fluid model in the linear stage in 1D cases<sup>[31,32]</sup>. For simplicity, two driver laser beams in the theoretical analysis are assumed to have constant intensities, and they propagate oppositely along the positive or negative  $y$ -axis into a homogeneous plasma. Using the normalized laser vector potentials  $\mathbf{a}_{1,2} = e\mathbf{A}_{1,2}/mc^2$ , the total vector potential of the driver laser beams becomes

$$\mathbf{a} = a_1 \cos(k_1 y - \omega t) \mathbf{e}_x + a_2 \cos(k_2 y + \omega t) \mathbf{e}_x. \quad (1)$$

Here, the two driver laser beams have the same frequency  $\omega_{1,2} = \omega_0$ , and the same wave number in the plasma  $k_{1,2} = \sqrt{1 - n_0/n_c} \omega_0/c$ , where  $n_0$  is the initial plasma density,  $n_c = \omega_0^2 \varepsilon_0 m_e / e^2$  is the critical plasma density corresponding to the laser frequency  $\omega_0$ ,  $\varepsilon_0$  is the permittivity of free space and  $m_e$  and  $e$  are the electron mass and charge, respectively. For a linearly polarized laser, its normalized vector potential  $a$  is related to its intensity  $I$  as  $I$  [W/cm<sup>2</sup>] =  $1.37 \times 10^{18} \cdot a^2 / \lambda^2$  [ $\mu\text{m}^2$ ], where  $\lambda$  is the laser wavelength in a vacuum. The intersection of two driver laser pulses will result in a periodic modulation in the total light amplitude and thus induce the following periodic ponderomotive force:

$$\mathbf{F}_p = m_e c^2 a_1 a_2 k_1 \sin(2k_1 y) \mathbf{e}_y. \quad (2)$$

Driven by such a ponderomotive force, the electron density will be modified firstly. Then, the ions will follow the electrons due to the charge-separation field. Finally, a periodic plasma density structure that is termed as the PDG will be induced. In the linear growth stage, the density perturbation of the PDG can be estimated as follows:

$$\delta n_e = - \left( 2k^2 c^2 / \omega_p^2 \right) a_1 a_2 \cos(2k_1 y) [1 - \cos(\omega_p t)], \quad (3)$$

where  $\omega_p$  is the plasma frequency. After the linear growth stage, however, the saturation, collapse and regrowth of the PDG will take place<sup>[32,33]</sup>. Further, the formed PDG will be nonuniform, since the driver laser beams always have finite durations and spot sizes in reality.

To illuminate the complicated dynamics of the PDG, a 2D particle-in-cell (PIC) simulation is conducted using the Osiris code<sup>[34]</sup>. The simulation box is  $[-200\lambda \leq x \leq 200\lambda] \times [-160\lambda \leq y \leq 160\lambda]$ , which is divided into  $6400 \times 5120$  cells. The plasma is located in  $[-200\lambda \leq x \leq 200\lambda] \times [-150\lambda \leq y \leq 150\lambda]$  and it has a uniform electron number density  $n_e = 0.3n_c$  in the region  $-195\lambda \leq x \leq 195\lambda$  and a  $5\lambda$  rising or falling ramp at each side in the  $x$  direction. For the plasma region, 16 macro-particles per cell are allocated. The plasma is assumed initially to be cold and the ions are the protons with  $m_p = 1836m_e$ . Two Gaussian driver laser pulses are incident along the positive or negative  $y$ -axis, respectively. They are p-polarized (the electric fields along the  $x$  direction) with a wavelength  $\lambda = 1 \mu\text{m}$ . These two driver pulses are assumed to have the same normalized amplitude  $a_1 = a_2 = 0.02$ , the same spot size (full width at half maximum (FWHM) in intensity) of  $100 \mu\text{m}$  and the same FWHM duration of  $150T_0$ . It is assumed that the peaks of the driver laser pulses will arrive at the simulation box center at  $t = 0$  if there is no plasma, and the simulation begins at  $t = -460T_0$ .

The PDG structure at  $t = 590T_0$  is displayed in Figure 2(a), where an obvious modulation in the plasma density is evidenced for the laser intersecting region. Zooming into

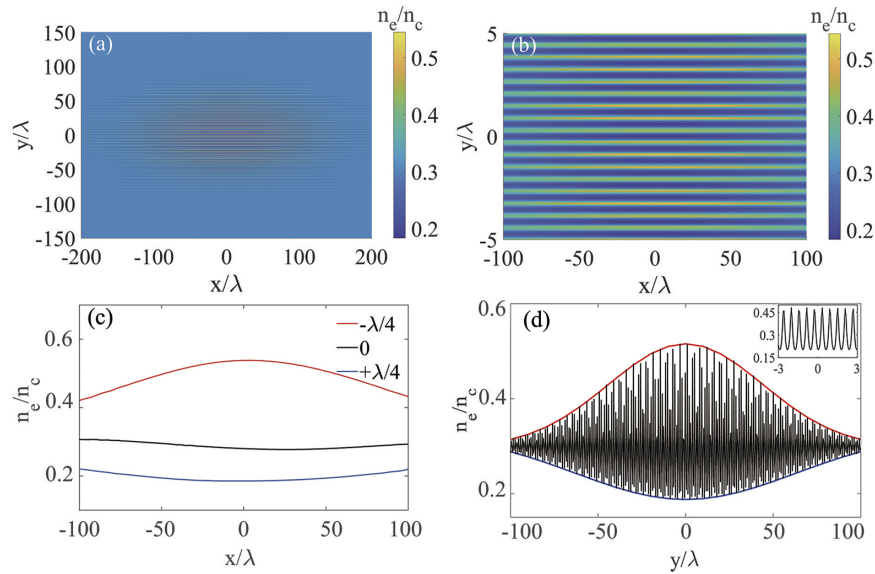


**Figure 2.** The electron density distribution of (a) the overall plasma region and (b) the center region  $[-100\lambda \leq x \leq 100\lambda] \times [-5\lambda \leq y \leq 5\lambda]$  at  $t = 590T_0$ , respectively. (c) The corresponding electron density profiles along the  $x$  direction at  $y = -\lambda/4, 0, \lambda/4$ , respectively. Here,  $y = \pm\lambda/4$  are roughly along the plasma density trough and peak, respectively. (d) The corresponding electron density profiles along the  $y$  direction at  $x = 0$ , in which the inset displays the enlarged density profile in the region  $-3\lambda < y < 3\lambda$ . The upper and lower envelopes of this density profile are also outlined by the red and blue curves, respectively.

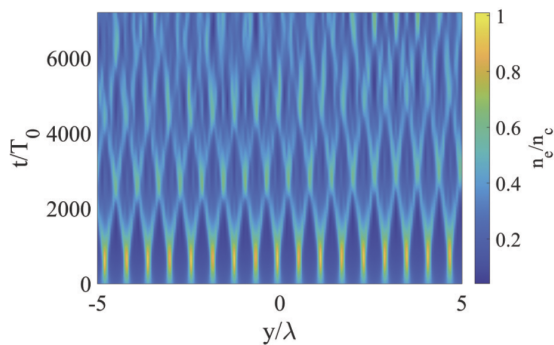


**Figure 3.** The time evolution of the electron density profile along the  $y$ -axis. Note that the PDG experiences a time periodic process of formation, saturation and collapse. The simulation parameters are the same as those in Figure 2.

the center region  $[-100\lambda \leq x \leq 100\lambda] \times [-5\lambda \leq y \leq 5\lambda]$ , Figure 2(b) illustrates that the density modulation has a clear periodicity along the  $y$  direction with a wavelength close to the laser wavelength in the plasma. However, Figure 2(c) shows that the density modulation in the  $x$  direction will be nonuniform and confined in a finite region, since the driver laser beams have finite spot sizes. Here, the peak and trough of the PDG are roughly achieved at  $y = \mp\lambda/4$ , respectively. Furthermore, Figure 2(d) shows that the density modulation in the  $y$  direction is also nonuniform.

More importantly, the plasma density modulation will be time-dependent. The time evolution of the plasma density profile along the  $y$ -axis is displayed in Figure 3. It is illustrated that the peak density of the PDG increases gradually to a maximum value in the first development stage. Then

the PDG will saturate and collapse due to the ion wave breaking<sup>[32,33]</sup>. Interestingly, the formation of the PDG will restart again after its collapse. As shown in Figure 3, the formation, saturation and collapse of the PDG could take place for several rounds. Due to its spatial nonuniformity and temporal evolution, the PDG will induce a complicated modulation upon the laser pulse passing through it. The laser depolarization by such a complicated and changeable PDG will be illuminated in the following paragraphs.

### 3. Depolarization of the laser pulse

The propagation of an electromagnetic wave through the PDG is similar to the electron movement in crystalline solids. Therefore, the theory of energy bands in solid physics can be employed for the theoretical analysis of the laser propagation through the PDG. For simplification, the PDG is assumed to be composed of alternating high- and low-density layers. Each high-density layer has a uniform density  $n_h$  and a thickness  $l_h$ , and each low-density layer has a uniform density  $n_l$  and a thickness  $l_l$ . For keeping the plasma quasi-neutral, the relationship  $n_0 l = n_h l_h + n_l l_l$  is satisfied, where  $l = l_h + l_l$  is the periodic length of the PDG. For a spatially infinite PDG, the dispersion relation for the s-polarized (transverse electric (TE) mode) wave is given by the following:

$$\cos(kl) = \cos(k_h l_h) \cos(k_l l_l) - \frac{1}{2} \left( \frac{k_l}{k_h} + \frac{k_h}{k_l} \right) \sin(k_h l_h) \sin(k_l l_l), \tag{4}$$

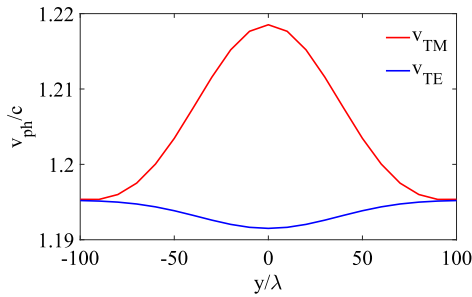


**Figure 4.** The phase velocities of the s-polarized ( $v_{TE}$ ) and p-polarized ( $v_{TM}$ ) light waves obtained from Equations (4) and (5), respectively, in which the electron density profile presented in Figure 2(d) is employed.

while for the p-polarized (transverse magnetic (TM) mode) wave it is given by the following:

$$\cos(kl) = \cos(k_h l_h) \cos(k_l l_l) - \frac{1}{2} \left( \frac{n_l^2 k_l}{n_h^2 k_h} + \frac{n_h^2 k_h}{n_l^2 k_l} \right) \sin(k_h l_h) \sin(k_l l_l), \quad (5)$$

where  $k$  is the laser wave number in the PDG when it propagates along the layers,  $k_h = (\omega/c) \sqrt{1 - n_h/n_c}$  and  $k_l = (\omega/c) \sqrt{1 - n_l/n_c}$ .

Due to their different dispersion relations, the s- and p-polarized electromagnetic waves will have different phase velocities. More importantly, the phase velocity difference will vary in both time and space as long as the PDG is spatially nonuniform and temporally variable. Using the electron density profile presented in Figure 2(d), the phase velocity of the s- and p-polarized light waves along the y-axis can be obtained according to Equations (4) and (5), respectively. The results are displayed in Figure 4, in which the phase velocity difference is clearly illustrated and it is nonuniform along the y-axis. Consequently, the final phase difference between the s- and p-polarized light waves will be proportional to the integral of the phase velocity difference over time, as follows:

$$\Delta\phi = \int_0^l k \frac{v_{TM}(x) - v_{TE}(x)}{v_{TE}(x)} dl. \quad (6)$$

Since the phase velocity difference varies in time and space, the resultant phase difference between the s- and p-polarized light components of a probe laser pulse will also change with time and space. Therefore, the final polarization state of the probe laser pulse that initially has both non-zero s- and p-polarized light components will vary in both space and time. That is to say, the probe laser pulse will be depolarized by the dynamic PDG.

To illuminate the laser depolarization by the dynamic PDG, some additional PIC simulations are conducted. In the first simulation, the parameters of two driver laser pulses and the initial plasma are the same as those used in Figure 3.

In addition to two driver laser pulses, a probe laser pulse whose polarization plane is oriented at  $45^\circ$  with respect to the  $x$ - $y$  plane is incident along the  $x$ -axis into the PDG. The probe laser pulse has Gaussian intensity profiles in both the longitudinal and transverse directions, it has the peak intensity  $a_0 = 0.05$ , the wavelength  $\lambda = 1 \mu\text{m}$ , the focal FWHM spot size of  $100 \mu\text{m}$  and the FWHM duration  $\tau = 200T_0$ . The peak of the probe laser pulse is assumed to arrive at  $(x, y) = (0, 0)$  at  $t = 515T_0$  if there is no plasma, that is, it is delayed by  $515T_0$  in time with respect to the driver laser pulses.

To describe the laser polarization state, the Stokes parameters  $I$ ,  $Q$ ,  $U$  and  $V$  are introduced<sup>[35]</sup>. Here  $I = |E_y|^2 + |E_z|^2$  denotes the intensity regardless of polarization,  $Q = |E_y|^2 - |E_z|^2$  denotes the linear polarization along the  $y$ (+)- or  $z$ (-)-axis,  $U = 2\text{Re}\{E_y^* E_z\}$  denotes the linear polarization at  $+45^\circ$  (+) or  $-45^\circ$  (-) from the  $y$ -axis and  $V = 2\text{Im}\{E_y^* E_z\}$  denotes the right-handed (+) or left-handed (-) circular polarization, where  $E_y$  ( $E_z$ ) is the complex amplitude of the electric field along the  $y$ ( $z$ )-axis and  $E_y^*$  is the complex conjugate of  $E_y$ . It is worth pointing out that the probe laser pulse initially has  $U = I$  and  $Q = V = 0$ , since it is linearly polarized at  $+45^\circ$  with respect to the  $y$ -axis. This implies that the s- and p-polarized light components of the probe laser are in phase and of the same amplitude at the beginning.

During the probe laser propagation in the PDG, its s- and p-polarized light components gradually become out of phase due to their different phase velocities. More importantly, the phase difference between them varies in time and space. As a result, the Stokes parameter distributions of the probe laser pulse become very complicated after it passes through the PDG, as shown in Figure 5. Above all, the parameters  $Q$  and  $V$  are no longer zero. Moreover, there are periodic variations in the parameters  $U$  and  $V$ . Further, the longitudinal (at  $y = 0$ ) and transverse (at  $x = 425\lambda$ ) profiles of the Stokes parameters are displayed in Figures 6(a) and 6(b), respectively. All of these illustrate that the polarization state of the probe laser becomes variable in both time and space after it passes through the PDG.

For the Stokes parameters, they always satisfy  $Q^2 + U^2 + V^2 \leq I^2$ , where the equality is achieved for fully polarized lights. For partially polarized lights,  $0 < (Q^2 + U^2 + V^2) / I^2 < 1$ . It is worth pointing out that  $Q^2 + U^2 + V^2 = I^2$  is satisfied at every infinitely small point in Figure 5. If the parameters  $I$ ,  $Q$ ,  $U$  and  $V$  are averaged over the longitudinal or transverse directions, however, the following averaged polarization degree

$$P_{t,l} = \sqrt{\langle Q \rangle_{l,t}^2 + \langle U \rangle_{l,t}^2 + \langle V \rangle_{l,t}^2} / \langle I \rangle_{l,t}$$

will be obviously smaller than one, where  $\langle \dots \rangle_{l,t}$  represents the average over the longitudinal (l) or transverse (t)

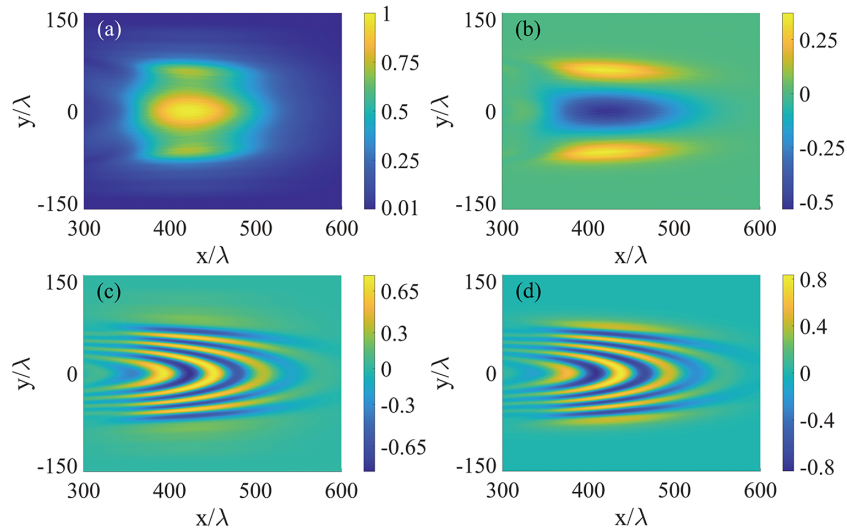


**Figure 5.** The spatial distributions of the Stokes parameters (a)  $I$ , (b)  $Q$ , (c)  $U$  and (d)  $V$  of the probe laser pulse at  $t = 940T_0$  after it passes through the PDG. Here, all Stokes parameters are normalized to the instantaneous maximum laser intensity  $I_{\max}$ . The simulation parameters are given in the text.

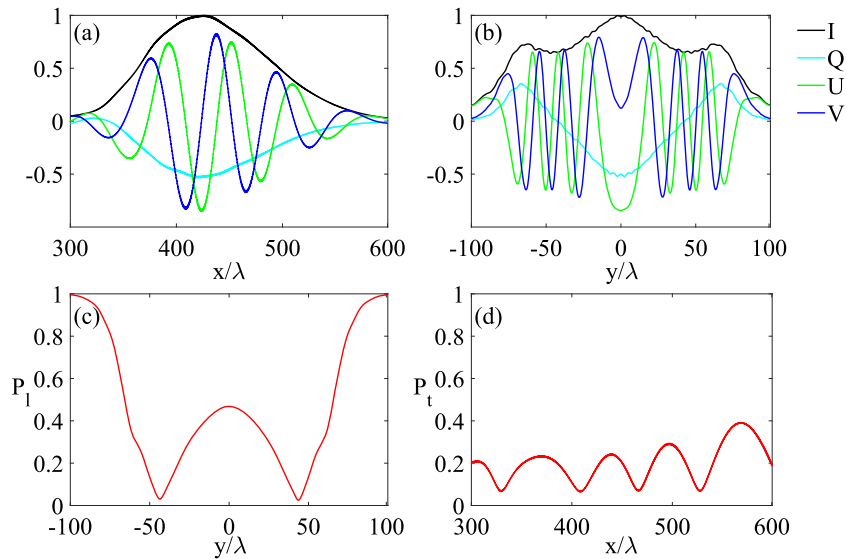


**Figure 6.** (a) Longitudinal profiles of the Stokes parameters at  $y = 0$  and (b) transverse profiles of the Stokes parameters at  $x = 425\lambda$ . (c) Longitudinally averaged polarization degree  $P_1$  and (d) transversely averaged polarization degree  $P_t$ . The simulation parameters are the same as those in Figure 5.

directions. Figure 6(c) shows that the longitudinally averaged polarization degree  $P_1$  is lower than 0.5 in the near-axis region  $|y| \leq 50\lambda$ , while Figure 6(d) shows that the transversely averaged polarization degree  $P_t$  is less than 0.4 in the whole pulse duration. These indicate that the temporal and spatial variations of the polarization state induced by the PDG are equivalent to a decrease of the averaged polarization degree. Moreover, Figure 6(c) indicates that the longitudinally averaged polarization degree  $P_1$  is nonuniform in the transverse direction since the depth of the PDG is nonuniform. Further, the transverse distribution of the PDG depth varies from time to time, which strongly depends on the durations of the driver laser pulses as well as the time delay between the driver laser pulses and the probe laser pulse.

In the above analysis, the PDG is induced by two counter-propagating driver laser pulses, and the probe laser is incident along the direction orthogonal to the driver lasers. Actually, the PDG can also be induced by two intersecting driver laser pulses with an intersection angle  $\varphi$ , as shown in Figure 7. In this case, the interference term of two intersecting driver laser pulses can be written as follows:

$$\mathbf{a}_1 \cdot \mathbf{a}_2 = \frac{a_1 a_2 \cos \varphi}{2} \left[ \cos \left( 2\omega t - 2kx \cos \frac{\varphi}{2} \right) + \cos \left( 2ky \sin \frac{\varphi}{2} \right) \right], \quad (7)$$

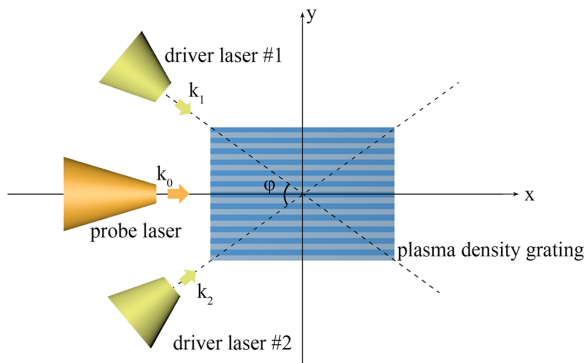


**Figure 7.** Laser depolarization by the PDG that is induced by two intersecting laser pulses with an intersection angle  $\varphi$ .

where the second term on the right-hand side induces the formation of the PDG. According to Equation (7), the periodic length of the PDG is related to the angle as  $l = \lambda / [2 \sin(\varphi/2)]$ , except that the PDG generated in this case is similar to that generated by two counter-propagating lasers, as shown in Figures 2 and 3. The formed PDG in this case can also be employed to depolarize the probe laser pulse. In addition, this scenario may spontaneously take place in the beam-crossing region in either indirect- or direct-drive ICF schemes if the polarizations and incident angles of the laser beams are arranged properly<sup>[26,27]</sup>.

To investigate the laser depolarization in the beam-crossing region, an additional PIC simulation is performed. In the simulation, a plasma with a uniform density  $n_0 = 0.27n_c$  is located in  $[-75\lambda \leq x \leq 75\lambda] \times [-400\lambda \leq y \leq 400\lambda]$ . The simulation box located within  $[-125\lambda \leq x \leq 425\lambda] \times [-400\lambda \leq y \leq 400\lambda]$  is resolved with 16 cells per wavelength, and 16 macro-particles are

initially allocated per cell. Two driver laser pulses #1 and #2 are incident into the plasma at angles of  $\varphi/2 = \pm\pi/4$  with respect to the  $x$ -axis, respectively. Two driver laser pulses are p-polarized (the electric fields are oriented in the  $x$ - $y$  plane). A probe laser pulse whose polarization plane is oriented at  $45^\circ$  with respect to the  $x$ - $y$  plane is incident along the  $x$ -axis into the plasma. All laser pulses have spatio-temporal Gaussian intensity profiles, the same wavelength of  $\lambda = 1 \mu\text{m}$  and the same normalized amplitude  $a_0 = a_1 = a_2 = 0.0468$ . Two driver laser pulses are assumed to have the same FWHM spot size of  $200\lambda$  and the same FWHM duration of  $200T_0$ . The probe laser pulse is assumed to have the FWHM spot size of  $100\lambda$  and the FWHM duration of  $150T_0$ . It is assumed that if there is no plasma the peaks of the driver laser pulses and the probe laser pulse will arrive at  $(x, y) = (0, 0)$  at  $t = 0$  and  $t = 370T_0$ , respectively. The simulation begins at  $t = -305T_0$ .

Analogous to Figure 5, Figure 8 shows that the Stokes parameter distributions of the probe laser pulse become very complicated after it passes through the PDG in this case. The periodic variations in parameters  $U$  and  $V$  are clearly illustrated in Figures 8(c) and 8(d), respectively. Such periodic variations in the Stokes parameters are also shown by the longitudinal (at  $y = 0$ ) and transverse (at  $x = 295\lambda$ ) profiles of the Stokes parameters in Figures 9(a) and 9(b), respectively. Moreover, Figure 9(c) shows that the longitudinally averaged polarization degree  $P_l$  is lower than 0.2 in the region  $|y| \leq 100\lambda$ , whereas Figure 9(d) shows that the transversely averaged polarization degree  $P_t$  is about 0.6 in the whole pulse duration. This demonstrates that the PDG can be induced not only by two counter-propagating laser pulses but also generally by two intersecting laser pulses with an intersection angle  $\varphi$ . The latter may be spontaneously

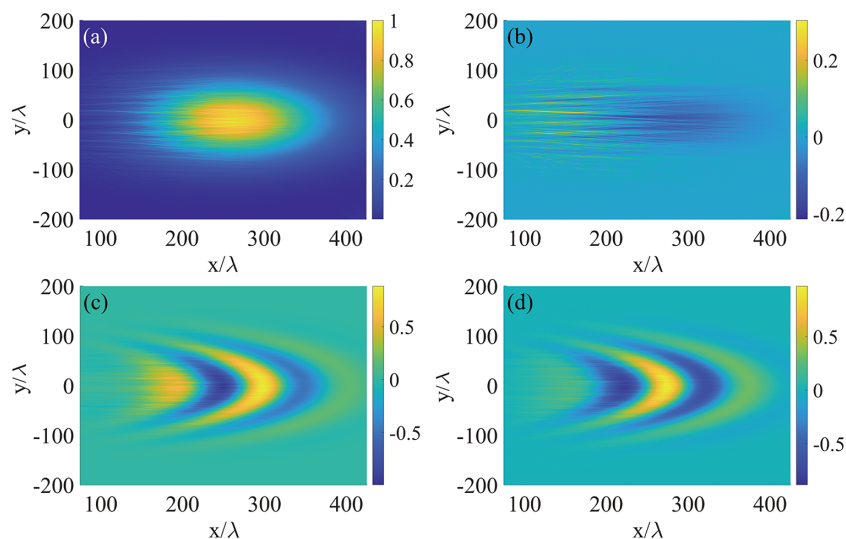


**Figure 8.** The spatial distributions of the Stoke parameters (a)  $I$ , (b)  $Q$ , (c)  $U$  and (d)  $V$  of the probe laser pulse at  $t = 650T_0$  after it passes through the PDG that is induced by two intersecting laser pulses with an intersection angle  $\varphi$ . Here, all Stokes parameters are normalized to the instantaneous maximum laser intensity  $I_{\text{max}}$ . The simulation parameters are given in the text.

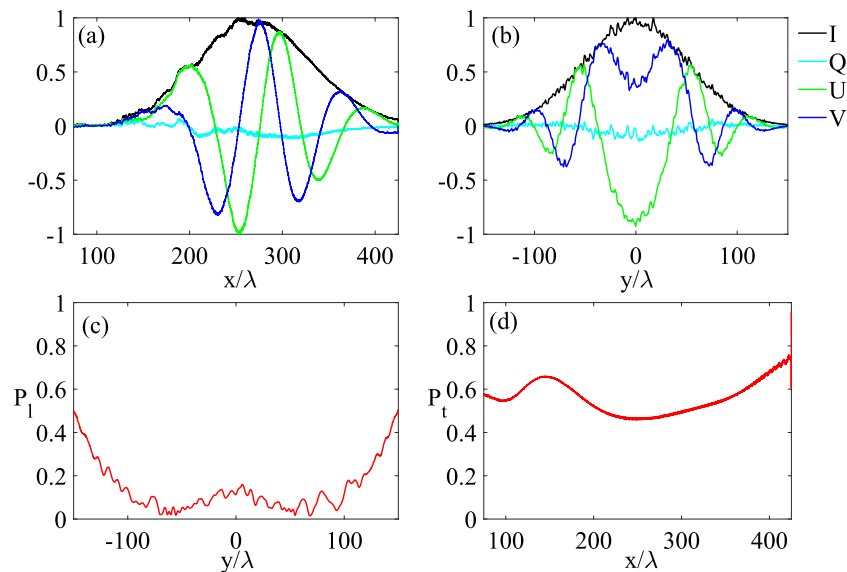


**Figure 9.** (a) Longitudinal profiles of the Stokes parameters at  $y = 0$  and (b) transverse profiles of the Stokes parameters at  $x = 295\lambda$ . (c) Longitudinally averaged polarization degree  $P_1$  and (d) transversely averaged polarization degree  $P_t$ . The simulation parameters are the same as those in Figure 8.

encountered for the crossed laser beams in ICF plasmas. The formed PDG will in turn modulate the polarization state of the laser beams, and consequently reduce their polarization degree.

#### 4. Discussion and conclusions

Since the normalized parameters are used in the simulations, such a dynamic PDG can in principle be used to depolarize the intense laser pulses at any wavelength. However, the density of the employed background plasma should increase for a shorter laser wavelength, which is often used in ICF. Correspondingly, collisional absorption may become the dominant process in a denser plasma. Fortunately, laser energy deposition via the collisional absorption usually is of benefit to ICF<sup>[36]</sup>. In addition, we find that the plasma temperature will increase gradually. Correspondingly, the peak density of the PDG will decrease due to the enhanced thermal pressure<sup>[32,33]</sup>. This may finally set a limitation on the use of dynamic PDGs in hot plasmas. On the other hand, it is worth noting that the theoretical growth rates of parametric instabilities will be reduced due to the enhanced Landau damping in plasmas with high temperatures<sup>[37]</sup>.

For the application of dynamic PDGs, the time-scale in which the polarization of the probe laser pulse becomes altered is a crucial factor. As shown in Figure 6(a), the dynamic PDG can make the polarization of the probe laser pulse vary obviously within a few tens of laser wave periods ( $\sim 0.2$  ps), while the stimulated Raman scattering (SRS) growth time in a homogenous plasma is also about 0.2 ps for the laser intensities of the order of  $10^{14}$  W/cm<sup>2</sup> that are usually employed in ICF<sup>[38]</sup>. In general, the growth time of the stimulated Brillouin scattering (SBS) is much longer than

that of the SRS. Therefore, one can expect that the laser depolarization via the dynamic PDG will play an important role in mitigating parametric instabilities such as SRS and SBS in ICF.

The time-scale in which the probe laser polarization is varied strongly depends on the typical variation time of the PDG. Further, it would decrease with the increase of the depth of the PDG (or the maximal achievable peak ion density). Moreover, it would also decrease with the increase of the width of the PDG, that is, the span of the PDG in the  $x$ -direction in the simulations. The latter is normally determined by the spot size of the driver laser pulses. However, it is difficult to give a formula for the time-scale in which the probe laser polarization is varied.

Concerning the variation time of the PDG, we have studied its dependence on the laser and plasma parameters by a series of 1D PIC simulations. As shown in Figure 10(a), we find that the saturation time  $T_s$  of the PDG decreases obviously with the increasing laser intensity  $a_0$  for a given initial plasma density  $n_0 = 0.3n_c$ . Here, the saturation time  $T_s$  is defined as the time required to achieve the maximal peak ion density. However, the maximal achievable peak ion density  $n_{\max}$  is nearly unchanged with the increasing  $a_0$ . On the other hand, Figure 10(b) shows that the saturation time  $T_s$  of the PDG increases slightly with the increasing plasma density  $n_0$  for a given laser intensity  $a_0 = 0.02$ , while the maximal achievable peak ion density  $n_{\max}$  increases obviously with the increasing plasma density  $n_0$ .

Based on the above analysis, one can see that the intensities and spot sizes of the driver laser pulses and the initial plasma density will combine to set a minimum time-scale in which the probe laser polarization can be varied. In general, the time-scale in which the probe laser polarization

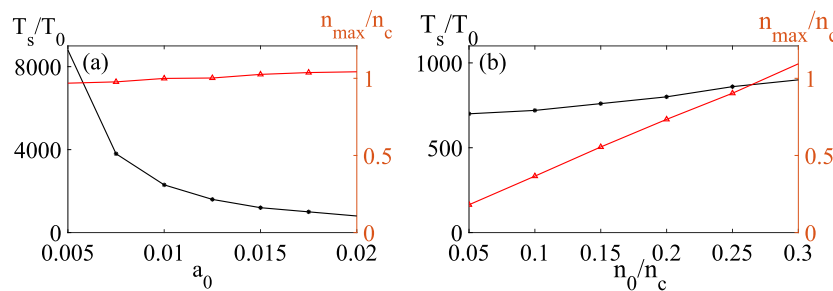


**Figure 10.** The saturation time  $T_s$  (black solid lines) and the maximal achievable ion density  $n_{\max}$  (red solid lines) as functions of (a) the laser intensity  $a_0$  for a given initial plasma density  $n_0 = 0.3n_c$  and (b) the initial plasma density  $n_0$  for a given laser intensity  $a_0 = 0.02$ . Except for the laser intensities and initial plasma densities, other laser–plasma parameters are the same as those used in Figure 5.

is varied is expected to decrease with the increase of the initial background plasma density as well as the increase of the intensity and spot size of the driver laser pulses.

In summary, we have shown that the PDG induced by two intersecting driver laser pulses is not only nonuniform in space but also varies over time. Such a dynamic PDG can induce a modulation upon the polarization state of the probe laser pulse passing through it. The time-scale in which the probe laser polarization is varied depends on the initial background plasma density, as well as the intensities and spot sizes of the driver laser pulses. The polarization degree of the probe laser that is averaged over either the longitudinal or transverse direction will be greatly reduced, that is, the probe laser pulse is depolarized by the dynamic PDG. The depolarized laser beams may play an important role in mitigating parametric instabilities relevant to laser-driven ICF. More importantly, the scenario of laser depolarization may spontaneously take place for crossed laser beams that are employed as the drivers in either indirect- or direct-drive ICF schemes.

## Acknowledgement

This work was supported by the National Natural Science Foundation of China (Grant Nos. 11975154, 11991074, 12005287 and 12135009), the Strategic Priority Research Program of Chinese Academy of Sciences (Grant Nos. XDA25050100 and XDA25010100), the Presidential Foundation of the China Academy of Engineering Physics (Grant No. YZJLX2016008) and the Science Challenge Project (Grant No. TZ2018005). Simulations have been carried out on the Pi supercomputer at Shanghai Jiao Tong University.

## References

1. D. Strickland and G. Mourou, *Opt. Commun.* **55**, 447 (1985).
2. C. N. Danson, C. Haefner, J. Bromage, T. Butcher, J.-C. F. Chanteloup, E. A. Chowdhury, A. Galvanauskas, L. A. Gizzi, J. Hein, D. I. Hillier, N. W. Hopps, Y. Kato, E. A. Khazanov, R. Kodama, G. Korn, R. Li, Y. Li, J. Limpert, J. Ma, C. H. Nam, D. Neely, D. Papadopoulos, R. R. Penman, L. Qian, J. J. Rocca, A. A. Shaykin, C. W. Siders, C. Spindloe, S. Szatmári, R. M. G. M. Trines, J. Zhu, P. Zhu, and J. D. Zuegel, *High Power Laser Sci. Eng.* **7**, e54 (2019).
3. C. Radier, O. Chalus, M. Charbonneau, S. Thambirajah, G. Deschamps, S. David, J. Barbe, E. Etter, G. Matras, S. Ricaud, V. Leroux, C. Richard, F. Lureau, A. Baleanu, R. Banici, A. Gradinariu, C. Caldararu, C. Capiteanu, A. Naziru, B. Diaconescu, V. Iancu, R. Dabu, D. Ursescu, I. Dancus, C. A. Ur, K. A. Tanaka, and N. V. Zamfir, *High Power Laser Sci. Eng.* **10**, e21 (2022).
4. G. A. Mourou, T. Tajima, and S. V. Bulanov, *Rev. Mod. Phys.* **78**, 309 (2006).
5. K. A. Tanaka, K. M. Spohr, D. L. Balabanski, S. Balascuta, L. Capponi, M. O. Cernaianu, M. Cuciuc, A. Cucoanes, I. Dancus, A. Dhal, B. Diaconescu, D. Doria, P. Ghenuche, D. G. Ghita, S. Kisiov, V. Nastasa, J. F. Ong, F. Rotaru, D. Sangwan, P. A. Söderström, D. Stutman, G. Suliman, O. Tesileanu, L. Tudor, N. Tsoneva, C. A. Ur, D. Ursescu, and N. V. Zamfir, *Matter Radiat. Extremes* **5**, 024402 (2020).
6. B. C. Stuart, M. D. Feit, S. Herman, A. M. Rubenchik, B. W. Shore, and M. D. Perry, *Phys. Rev. B* **53**, 1749 (1996).
7. C. Thauray, F. Quéré, J. P. Geindre, A. Levy, T. Ceccotti, P. Monot, M. Bougeard, F. Réau, P. d'Oliveira, P. Audebert, R. Marjoribanks, and P. H. Martin, *Nat. Phys.* **3**, 424 (2007).
8. M. Nakatsutsumi, A. Kon, S. Buffechoux, P. Audebert, J. Fuchs, and R. Kodama, *Opt. Lett.* **35**, 2314 (2010).
9. V. M. Malkin, G. Shvets, and N. J. Fisch, *Phys. Rev. Lett.* **82**, 4448 (1999).
10. R. M. G. M. Trines, F. Fiúza, R. Bingham, R. A. Fonseca, L. O. Silva, R. A. Cairns, and P. A. Norreys, *Nat. Phys.* **7**, 87 (2011).
11. A. A. Andreev, C. Riconda, V. T. Tikhonchuk, and S. Weber, *Phys. Plasmas* **13**, 053110 (2006).
12. M. R. Edwards, J. M. Mikhailova, and N. J. Fisch, *Phys. Rev. E* **96**, 023209 (2017).
13. S. Weng, Q. Zhao, Z. Sheng, W. Yu, S. Luan, M. Chen, L. Yu, M. Murakami, W. B. Mori, and J. Zhang, *Optica* **4**, 1086 (2017).
14. Y. Shi, H. Qin, and N. J. Fisch, *Phys. Rev. E* **95**, 023211 (2017).
15. X. L. Zheng, S. M. Weng, H. H. Ma, Y. X. Wang, M. Chen, P. McKenna, and Z. M. Sheng, *Opt. Express* **27**, 23529 (2019).
16. Z. Li, Z. Wu, Y. Zuo, X. Zeng, X. Wang, X. Wang, J. Mu, B. Hu, and J. Su, *Phys. Plasmas* **28**, 013107 (2021).
17. I. Y. Dodin and N. J. Fisch, *Phys. Rev. Lett.* **88**, 165001 (2002).
18. G. Lehmann and K. H. Spatschek, *Phys. Rev. E* **100**, 033205 (2019).
19. M. R. Edwards, V. R. Munirov, A. Singh, N. M. Fasano, E. Kur, N. Lemos, J. M. Mikhailova, J. S. Wurtele, and P. Michel, *Phys. Rev. Lett.* **128**, 065003 (2022).
20. G. Lehmann and K. H. Spatschek, *Phys. Rev. E* **97**, 063201 (2018).
21. H. C. Wu, Z. M. Sheng, and J. Zhang, *Appl. Phys. Lett.* **87**, 201502 (2005).

22. S. Monchocé, S. Kahaly, A. Leblanc, L. Videau, P. Combis, F. Réau, D. Garzella, P. D'Oliveira, P. Martin, and F. Quéré, *Phys. Rev. Lett.* **112**, 145008 (2014).
23. P. Michel, L. Divol, D. Turnbull, and J. D. Moody, *Phys. Rev. Lett.* **113**, 205001 (2014).
24. D. Turnbull, P. Michel, T. Chapman, E. Tubman, B. B. Pollock, C. Y. Chen, C. Goyon, J. S. Ross, L. Divol, N. Woolsey, and J. D. Moody, *Phys. Rev. Lett.* **116**, 205001 (2016).
25. G. Lehmann and K. H. Spatschek, *Phys. Rev. Lett.* **116**, 225002 (2016).
26. S. H. Glenzer, B. J. MacGowan, P. Michel, N. B. Meezan, L. J. Suter, S. N. Dixit, J. L. Kline, G. A. Kyrala, D. K. Bradley, D. A. Callahan, E. L. Dewald, L. Divol, E. Dzenitis, M. J. Edwards, A. V. Hamza, C. A. Haynam, D. E. Hinkel, D. H. Kalantar, J. D. Kilkenny, O. L. Landen, J. D. Lindl, S. LePape, J. D. Moody, A. Nikroo, T. Parham, M. B. Schneider, R. P. J. Town, P. Wegner, K. Widmann, P. Whitman, B. K. F. Young, B. Van Wonterghem, L. J. Atherton, and E. I. Moses, *Science* **327**, 1228 (2010).
27. P. Michel, L. Divol, E. A. Williams, S. Weber, C. A. Thomas, D. A. Callahan, S. W. Haan, J. D. Salmonson, S. Dixit, D. E. Hinkel, M. J. Edwards, B. J. Macgowan, J. D. Lindl, S. H. Glenzer, and L. J. Suter, *Phys. Rev. Lett.* **102**, 025004 (2009).
28. W. L. Kruer, S. C. Wilks, B. B. Afeyan, and R. K. Kirkwood, *Phys. Plasmas* **3**, 382 (1996).
29. I. Barth and N. J. Fisch, *Phys. Plasmas* **23**, 102106 (2016).
30. H. H. Ma, X. F. Li, S. M. Weng, S. H. Yew, S. Kawata, P. Gibbon, Z. M. Sheng, and J. Zhang, *Matter Radiat. Extremes* **6**, 055902 (2021).
31. Z. M. Sheng, J. Zhang, and D. Umstadter, *Appl. Phys. B* **77**, 673 (2003).
32. H. H. Ma, S. M. Weng, P. Li, X. F. Li, Y. X. Wang, S. H. Yew, M. Chen, P. McKenna, and Z. M. Sheng, *Phys. Plasmas* **27**, 073105 (2020).
33. H. Peng, C. Riconda, M. Grech, J. Q. Su, and S. Weber, *Phys. Rev. E* **100**, 061201 (2019).
34. R. A. Fonseca, L. O. Silva, F. S. Tsung, V. K. Decyk, W. Lu, C. Ren, W. B. Mori, S. Deng, S. Lee, T. Katsouleas, and J. C. Adam, *Lect. Notes Comput. Sci.* **2331**, 342 (2002).
35. J. Tinbergen, *Astronomical Polarimetry* (Cambridge University Press, Oxford, 1996).
36. S. Atzeni and J. Meyer-ter-Vehn, *The Physics of Inertial Fusion* (Clarendon Press, Oxford, 2004).
37. C. S. Liu, *High-Power Laser-Plasma Interaction* (Cambridge University Press, Oxford, 2019).
38. D. S. Montgomery, *Phys. Plasmas* **23**, 055601 (2016).